Open Access

Advances in Environmental and Engineering Research

LIDSEN Publishing Inc.

Original Research

Adsorption of Phosphate by Synthesized Silver/Calcium Oxide-Activated Carbon Nanocomposite

George William Nyakairu *, Mariam Onize Usman, Muhammad Ntale

Makerere University, College of Natural Sciences, School of Physical Sciences, Department of Chemistry, P.O. Box 7062, Kampala, Uganda; E-Mails: george.nyakairu@mak.ac.ug; mariam.usman@students.mak.ac.ug; muhammad.ntale@mak.ac.ug

* **Correspondence:** George William Nyakairu; E-Mail: george.nyakairu@mak.ac.ug

Academic Editor: Pei Sean Goh

Adv Environ Eng Res
2023, volume 4, issue 2
doi:10.21926/aeer.2302033

Received: February 24, 2023
Accepted: May 15, 2023
Published: May 24, 2023

Abstract

Developing adsorbents with appreciable morphology will create new approaches for better phosphate adsorption performance. This study aims to investigate the design of an adsorbent by impregnating silver nanoparticles (AgNPs) onto calcium oxide-activated carbon (CaO-AC). The Ag/CaO-AC nanocomposite was used as an adsorbent to remove phosphate. Batch adsorption studies were performed to evaluate the effects of adsorbent dose, initial phosphate concentration, contact time, and pH on removing phosphate from an aqueous solution. The optimized conditions were applied to a real wastewater sample. The optimum condition for phosphate adsorption on Ag/CaO-AC nanocomposite was at an adsorbent dose of 0.02 g, an initial phosphate concentration of 40 $mg{\cdot}L^{-1}$, an equilibrium contact time of 45 minutes, and pH 7. Pseudo-second-order proved to be more accurate in representing the data of phosphate adsorption onto Ag/CaO-AC nanocomposite. The adsorption isotherm fitted well on the Langmuir model with a maximum adsorption capacity of 77.4 $mg{\cdot}g^{-1}$. From the kinetics and isotherm studies, chemisorption was the primary adsorption mechanism through ion exchange and ligand exchange mechanisms. The results of this study show that Ag/CaO-AC nanocomposite is a promising adsorbent for removing phosphate from wastewater.

Keywords
Adsorption; isotherms; kinetics; nanocomposite; phosphate removal; wastewater

1. Introduction

Phosphate removal and recovery from wastewater have played a crucial role in managing aquatic ecosystems, such as reducing eutrophication. Eutrophication is a gradual process by which water bodies become enriched with nutrients (e.g., phosphates) and cause the excessive growth of algae, cyanobacteria, and aquatic plants [1]. It causes a hypoxic condition in water and subsequent reduction in the natural habitat of fish [2]. According to World Health Organization (WHO), phosphate concentration in drinking water should not exceed 2 $mg{\cdot}L^{-1}$. In comparison, phosphate concentration should not exceed 5 $mg{\cdot}L^{-1}$ for wastewater discharged into the river [3]. According to the United States Environmental Protection Agency (USEPA), phosphate concentration above the limit of 0.025 $mg{\cdot}L^{-1}$ can cause the occurrence of harmful algal blooms [4]. Wastewater originating from municipal homes has an average total phosphate content of 5-20 $mg{\cdot}L^{-1}$, of which 1-5 $mg{\cdot}L^{-1}$ is organic, and the remaining component is inorganic [2].

In wastewater, total phosphorus is either inorganic polyphosphates and orthophosphates from detergents and other household products or organically bound phosphates from physiological processes. The poly-phosphates and organically bound phosphates dissolve and get converted to orthophosphates by hydrolysis, depending on their types, water temperature, and pH [5]. The different form of orthophosphates in water depends on the pH and chemical species, such as H_3PO_4, $H_2PO_4^-$, HPO_4^{2-}, and PO_4^{3-}in which the most abundant form is $H_2PO_4^-$ [6]. Orthophosphates are of concern because it is the most abundant form of phosphate in wastewater and the state assimilated directly by algae. Recently, research has focused on the efficiency of treating wastewater effluents, particularly those containing a substantial amount of nutrients (phosphorus and nitrogen).

Conventional wastewater treatment technologies have been extensively studied, such as chemical precipitation, biological treatment, membrane filtration/separation, ion exchange, and adsorption [5]. Among these methods, adsorption technology in phosphate removal from wastewater has several advantages, such as ease of operation, fast, and effectiveness at low phosphate concentrations [7]. The critical factors influencing adsorption are the specific surface area, porosity, pore size distribution, surface reactivity, structure distribution, and the relative affinity of the adsorbent for the adsorbate [8]. Adsorption also offers the advantages of regeneration and recovery of the adsorbent and the adsorbate, thereby enhancing the reuse of the adsorbent and recycling of the adsorbate (phosphate), which is non-renewable.

The different adsorbents used for phosphate removal from water include; Aluminium modified biochar [9], Laterite soils, Black cotton soil, fuller's earth [10], and several materials loaded with lanthanum such as carboxymethyl konjac glucomannan loaded with lanthanum [11], silver nanoparticles (AgNPs) [12], silver nanoparticles-loaded activated carbon derived from tea residue (AgNPs-TAC) [13]. Different studies have used silver nanoparticles as adsorbents to remove phosphates and other pollutants in aqueous solutions and have shown high efficiency. However, the application of nanoparticles in wastewater treatments may be limited owing to their low

stability and great tendency to aggregate [14]. Furthermore, nanoparticles can easily leach into the water during treatment due to their small size in nanometers, making separation difficult. Therefore, modification is required by impregnating the nanoparticles onto support materials to increase their stability and ease the separation. For example, silver nanoparticles are coated onto some support such as sand, zeolite, and fiberglass to prevent the particles' agglomeration and enhance the removal of pollutants from treated water [15]. In addition, carbon-based materials such as activated carbon, graphene, graphene oxides, and carbon nanotubes are also studied as suitable nanoparticle support materials for water purification.

In a study by Khodadadi et al., 2017 [16], a nanomagnetic iron particle coated with powder-activated carbon was used to remove phosphate, and the maximum phosphate adsorption efficiency of 100 % was recorded at pH 2. Also, Iron/Cobalt chitosan-modified nano-particles gave 52.7 % and 58.7 % phosphate removal in synthetic wastewater and river water [17]. Cepan et al., 2021 [2] conducted comparative research on the adsorption performances of five different adsorbents (magnetite, cobalt ferrite, titanium dioxide, zinc oxide, zeolite) on phosphate removal from aqueous solution. The result showed that the adsorption efficiency of the materials was in the order: zinc oxide 51%, titanium dioxide 71%, cobalt ferrite 80%, magnetite 88%, and mordenite zeolite 96%. These results showed the high efficiency of mordenite-zeolite and magnetic materials in phosphate recovery from an aqueous solution.

In this study, AgNPs synthesized by the chemical reduction method were impregnated onto calcium oxide/activated carbon composite by taking advantage of the porosity of the activated carbon to form Ag/CaO-AC nanocomposite. Impregnation of silver nano-particles onto calcium oxide-activated carbon composite was to increase the specific surface characteristics, stability, and functional moieties of the nano-composite to give better phosphate removal. The study aimed to design an Ag/CaO-AC nanocomposite for phosphate adsorption from synthetic and real wastewater samples. Several experimental parameters that influence phosphate adsorption were investigated, such as the effects of adsorbent dose, initial phosphate concentration, contact time, and pH. Modified activated carbon with silver and calcium ions contain positively charged active sites, e.g., Ag^{+} and Ca^{2+}. Positive surface groups render the adsorbent capable of binding and adsorbing anionic species like phosphates.

2. Materials and Methods

2.1 Materials

All chemicals, including potassium dihydrogen phosphate (98.0%), silver nitrate (99.99%), sodium hydroxide, sodium borohydride (98%), ascorbic acid (95%), potassium antimonyl tartrate (99%), ammonium molybdate (98%), sulfuric acid (98%), were purchased from Sigma Aldrich. Activated carbon (95%), and starch were obtained from the laboratory. All chemicals were of analytical grade quality. The solutions were prepared in double distilled and deionized water using standard procedures.

2.2 Synthesis of Silver Nanoparticles

A silver nitrate (100 mL, 0.001 M) was mixed with starch (0.05 g) to produce a starch solution containing silver ions with constant stirring using a magnetic stirrer at 70 °C to ensure a homogenous

solution. The addition of starch in the preparation of silver nanoparticles produces stable and unaggregated nanoparticles. Sodium borohydride (25 mL, 0.001 M) was added gradually in drops into the mixture with constant stirring for some time to enhance the formation of silver nanoparticles. The solution was decanted and washed with deionized water using the method of Trinh et al., 2020 [13]. The resultant solution was cooled to room temperature and stored for further use. The following equations illustrate the process.

$$\mathrm{AgNO_3 + NaBH_4 \rightarrow Ag^0 + \frac{1}{2}H_2 + B_2H_6 + NaNO_3} \quad (1)$$

2.3 Synthesis of CaO-AC Composite

The CaO-AC composite synthesis involved dispersing the activated carbon (2 g) in deionized water (100 mL) at room temperature with $CaCO_3$ (5 g) at constant stirring for 5 hours. The sample was dried at 100 °C for 6 hours and calcined at a temperature of 850 °C for 3 hours in an inert atmosphere using the method of [18]. The calcined sample (CaO-AC composite) was stored for characterization and the impregnation process with silver nanoparticles.

2.4 Synthesis of Ag/CaO-AC Nanocomposite

The synthesis of the Ag/CaO-AC nanocomposite using the incipient wet impregnation method (loading the CaO-AC in solid form into a solution of silver nanoparticles) followed a procedure described by Trinh et al., 2020 [13]. The mixture of CaO-AC and AgNPs was prepared by adding CaO-AC onto a solution of Ag-NPs at various mass ratios (3%, 4%, 5%) in a 250 mL Erlenmeyer flask. The flask and its content were magnetically stirred for 24 hours. After the impregnation, the wet particles were filtered and dried for 5 hours at 105 ºC and then 60 ºC overnight to obtain the Ag/CaO-AC nanocomposite.

2.5 Characterization Techniques

UV-Visible spectrophotometer (JENWAY 7315 Spectrophotometer Model) investigated the confirmation of silver nanoparticle formation. The morphology and elemental composition in the CaO-AC synthesized Ag/CaO-AC were studied using SEM/EDS (JEOL JSM-648 with EDS from IXRF company). The crystalline phases were determined using an X-ray diffractometer (X'Pert Pro diffractometers) at the Faculty of Science and Technology, University of Silesia, Katowice.

2.6 Adsorption Measurements

Batch adsorption experiments were conducted to remove phosphates from synthetic solutions by the Ag/CaO-AC nanocomposite. A digital magnetic stirrer with a PT 1000 temperature sensor and a Teflon-coated magnetic stirring bar (length of 2 cm) was used to stir the phosphate solution with Ag/CaO-AC nanocomposite. The initial adsorption experiments with the nanocomposite obtained from the different mass ratios were performed to identify the optimum impregnation ratio of AgNPs and AC-CaO composite. In the experiment, 0.03 g of Ag/CaO-AC produced from the three impregnation ratios selected were added into 50 mL Erlenmeyer flasks containing a 25 mL solution of 10 $mg \cdot L^{-1}$ of phosphate in a sealed flask for 30 minutes at room temperature and the natural pH

of the solution. The liquid samples were left for some time to settle, decanted, and filtered through 0.45 µm filter paper before the analysis of the residual phosphate concentration.

A batch adsorption experiment of Ag/CaO-AC nanocomposite on phosphate removal by assessing the effects of adsorbent dose (0.05-0.6 g), initial concentration (10-80 $mg \cdot L^{-1}$), contact time (15-105 minutes), and pH (3-11) were conducted. In addition, the solution's pH level was adjusted using 1 M sodium hydroxide or 1 M hydrochloric acid solution using a digital pH meter (Consort pH meter C6010).

2.7 Determination of Equilibrium Phosphate Concentration

After the adsorption experiment, the liquid samples were filtered through 0.45 µm filter paper before analyzing the residual phosphate concentration. For one analysis, 5 mL of the filtrate was taken for the colorimetric assay three times. The sample's equilibrium concentration of phosphate ions was determined using a UV-Vis spectrophotometer at 880 nm. The adsorption capacities of Ag/CaO-AC nanocomposites for phosphorus adsorption at equilibrium q_e (in mg/g) and the percentage removal in mg/g were calculated by Equations 2 and 3.

$$Q_e = \frac{(C_o - C_e)V}{W} \tag{2}$$

$$\%\text{removal} = \frac{(C_o - C_e)}{C_o} \times 100 \tag{3}$$

where C_o ($mg \cdot L^{-1}$) is the initial phosphate concentration, C_e ($mg \cdot L^{-1}$) is the equilibrium concentration of phosphate, V is the phosphate solution volume (L), and W is the dry weight (g) of Ag/CaO-AC nanocomposite.

2.8 Data Analysis

The experimental data for the Adsorption kinetics were fitted using the pseudo-first-order and pseudo-second-order kinetic models. Langmuir and Freundlich isotherm models were used to model the adsorption isotherms.

2.9 Real Wastewater Sample Collection and Treatment

The real wastewater sample used in this study was collected from the Lubigi Sewage Treatment Plant, Uganda, to perform the phosphate removal experiment. The wastewater's effluent characteristics (pH, phosphate concentration, and electrical conductivity (EC) were determined. The representative sample was then transported to the Department of Chemistry, Makerere University, Uganda, and stored in a refrigerator at 4°C. The phosphate concentration in the real wastewater sample was determined using the UV-Visible spectrophotometer at 880 nm as described for the synthetic wastewater.

3. Results and Discussion

3.1 Characterization of Ag/CaO-AC Nanocomposite

The results of the characterization of the nanocomposites using UV-Visible spectroscopy, SEM/EDS, and XRD are discussed in this section.

3.1.1 Surface Plasmon Resonance of AgNPs

The surface plasmon resonance of AgNPs was determined using UV-Vis spectroscopy (JENWAY 7315 Spectrophotometer) with a wavelength range set between 350-600 nm. A volume of the prepared silver nanoparticles solution (5 mL) was taken, diluted with 5 mL of ultrapure water, and immediately taken for UV-Vis measurement. In the synthesized AgNPs, UV-Visible spectra (Figure 1) gave an absorption peak of silver nanoparticles at 420 - 430 nm. The maximum peak was assigned to the surface plasmon resonance of silver nanoparticles. The formation of bright yellow color during AgNP synthesis also confirms the formation of silver nanoparticles [19]. The surface plasmon resonance in silver nanoparticle solution is responsible for the absorption band. Most metal nanoparticles contain free electrons that give rise to the surface plasmon resonance; the mutual vibrations of the metal nanoparticles in resonance with the light cause the absorption band. AgNPs interact with light due to electrons' conduction, which causes collective oscillation of the free electrons at the metal surface layer when they are excited by light at a specific wavelength [20]. This absorption energy is highly dependent on the degree of plasmon resonance. It is likely to increase or decrease slightly for the ratio of silver ions to the zerovalent silver present in the solution [21].

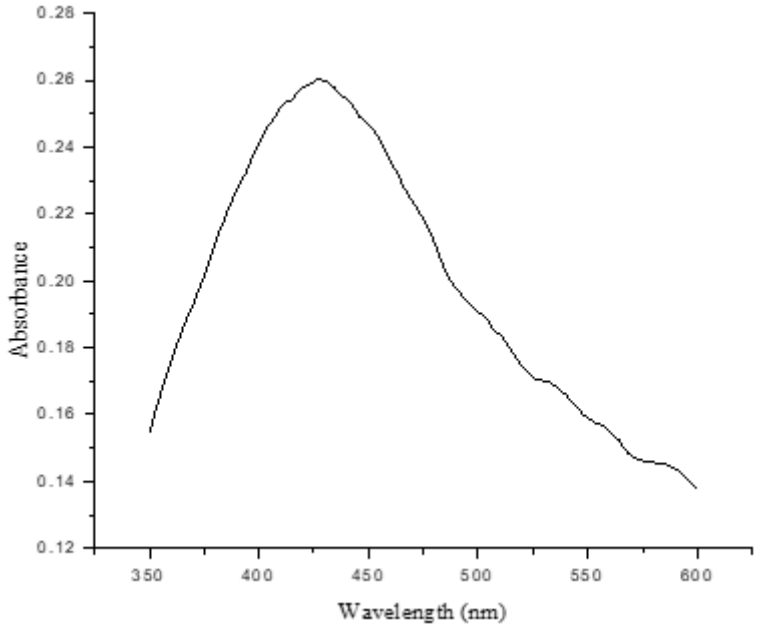

Figure 1 UV-Vis spectra of synthesized AgNPs showing the maximum absorption around 420 nm.

3.1.2 Morphology and Elemental Composition of Nanocomposites

One of the most important physical factors affecting an adsorbent's adsorption capacity is its surface morphology. Figure 2 gives the results from the SEM/EDS analysis. As shown in the image, the small white particles represented silver nanoparticles distributed on the surface of the CaO-AC due to the strong affinity of silver for oxygen groups in the functional groups of CaO-AC [14]. Nevertheless, after the phosphate adsorption experiment, the composition of Ag/CaO-AC showed the presence of phosphorus. This indicates that some phosphates have been adsorbed on the Ag/CaO-AC. Similar SEM/EDS analysis results were obtained for phosphate adsorption with AgNP-TAC [13].

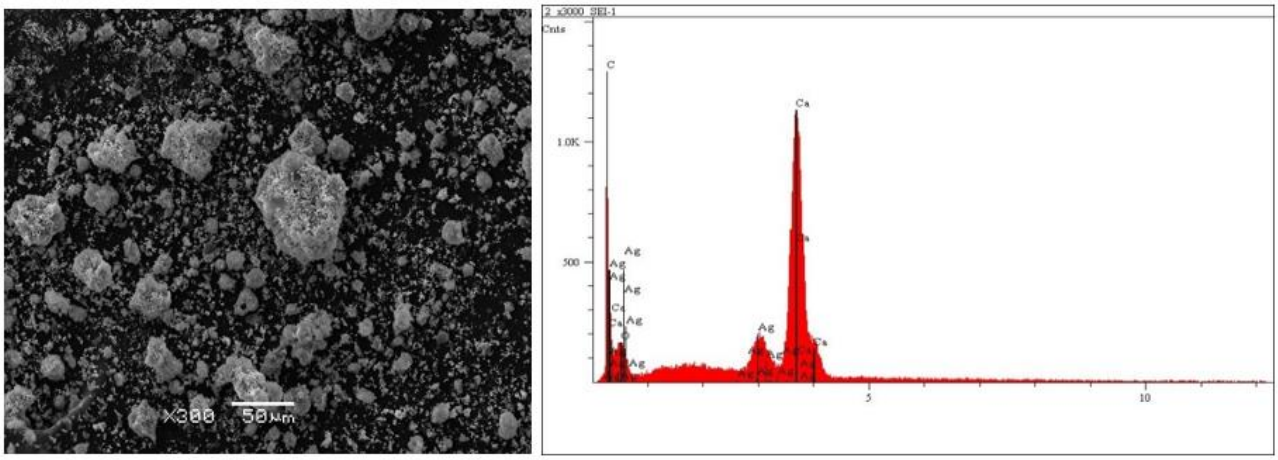

Figure 2 SEM/EDS analysis of the Ag/CaO-AC nanocomposite.

As determined by EDS, the elemental composition of the adsorbent before phosphate adsorption showed that the constituents of the Ag/CaO-AC were (C, O, Ca, and Ag) respectively. However, after the phosphate adsorption experiment, the composition of Ag/CaO-AC showed the occurrence of P in the EDS result (Figure 3). The presence of P is a clear indication of the adsorption of some phosphates on the Ag/CaO-AC. Trinh et al., 2020 [13] obtained similar SEM/EDS analysis results with the occurrence of P in the EDS result after phosphate adsorption. After the phosphate adsorption on the surface of the nano-composite, there seems to be tiny white crystal growth on the surface of the adsorbent. These tiny particles are likely to be calcium phosphate or hydroxyapatite formed on the surface of the CaO particles by continuously reacting with phosphate ions. This was discussed by Darshana Senarathna et al., 2020 [22] when they applied a vaterite polymorph of porous calcium carbonate nanoparticles to remove phosphate from solutions. The results obtained from the SEM/EDS analysis confirmed the modification of the Ag/CaO-AC and the adsorption of phosphate on the surface of the Ag/CaO-AC nano-composite.

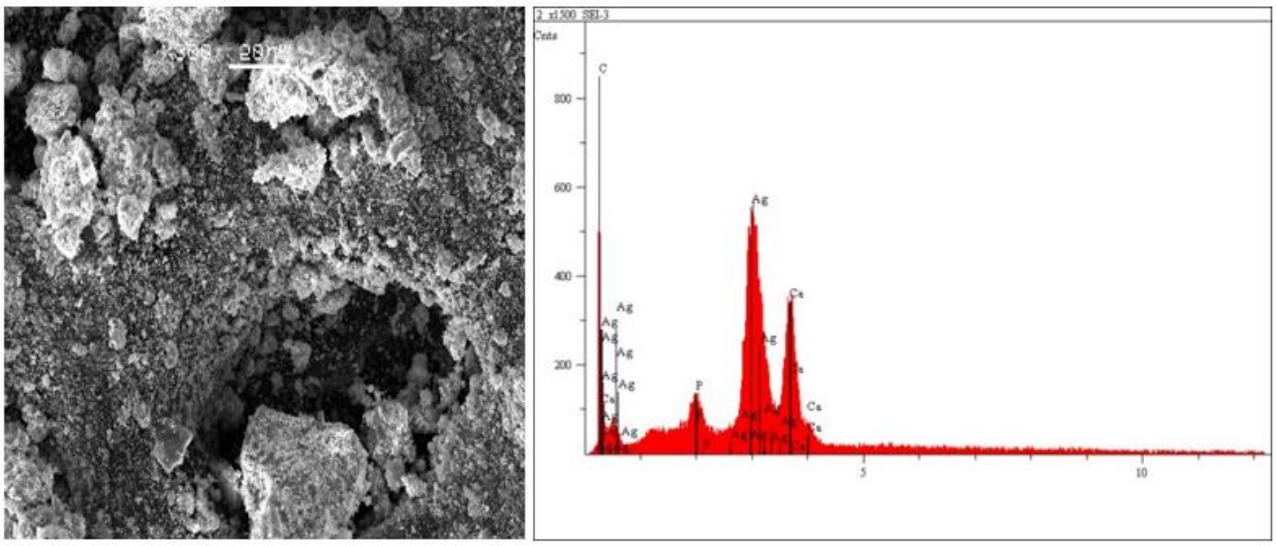

Figure 3 SEM/EDS analysis of the Ag/CaO-AC nanocomposite after phosphate adsorption.

3.1.3 X-ray Diffraction Pattern of Nanocomposites

XRD confirms and explores nanomaterials' crystal structures as a unique characterization technique. The crystallinity of CaO-AC and Ag/CaO-AC before and after phosphate adsorption in this study was determined using powdered XRD. The results of the XRD powder diffraction (Figure 4) indicated that the obtained nanocomposite was well crystallized. The observed peaks in the XRD also show the synthesized nanocomposite with various crystalline phases. The peaks at around 2θ of 29.47° and 43.23° in the diffractogram *a* for $CaCO_3$-AC are characteristic of calcium carbonate in the form of calcite [23]. After calcination, the reduction in the peak intensity and the formation of a new peak at 18.14° show the decomposition of the $CaCO_3$ and the formation of CaO, as shown in *b*. The peak at 18.14° may also represent $Ca(OH)_2$, possibly due to the reaction between CaO and H_2O in the air. The peaks at 26.82°, 32.99°, 38.26°, and 55.18°, and the increased peak intensities at 2θ of 47.21° and 65.76° confirmed the presence of AgNPs in the new Ag/CaO-AC nanocomposite as shown in *c*. A similar XRD peak was obtained from leaf extract and callus extract synthesized silver nanoparticles with peaks around 32.5°, 38.3°, 64.4°, and 64.5° [24]. The outcome of XRD of the sample after modification shows that after the impregnation of AgNPs on the surface of CaO-AC, the Ag/CaO-AC surface appeared to have AgNPs. This result is similar to the recent result obtained by Trinh et al., 2020 [13] by loading AgNPs on tea-activated carbon at the peaks of 37.88°. Generally, the peaks of AgNPs at 2θ of 47.21° and 65.76° suggest that the smaller silver nanoparticles are embedded in the support material (CaO-AC). Such a pattern confirms the silver nanoparticles' fabrication on CaO-AC [14].

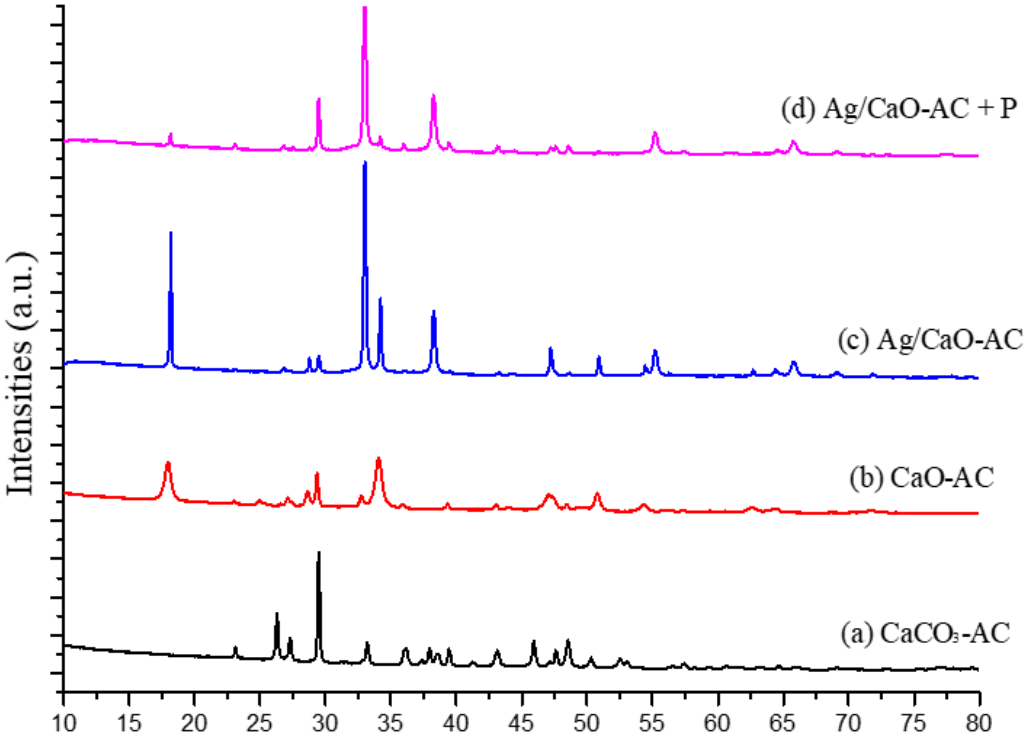

Figure 4 XRD results to show the nanocomposite's different crystallite phases at various synthesis stages. a) Uncalcined CaO-AC, b) calcined CaO-AC, c) Ag/CaO-AC nanocomposite before phosphate adsorption, d) Ag/CaO-AC nanocomposite after phosphate adsorption.

The XRD pattern of the nanocomposite after phosphate adsorption is shown in the last diffractogram *d*, with an observed change and reduction in the peak intensity, which might be due to the growth of certain crystal planes during phosphate adsorption. Most peaks were lost, and reduced intensity was observed due to phosphates' adsorption. Furthermore, the adsorption process could cause loss of the active sites of the adsorbent, causing the reduction in the crystallinity hence, the reduction in peak intensity. Additionally, the peak intensity around 29.47° increased, probably due to the formation of the calcium phosphate phase after the phosphate adsorption. This pattern explains the coating of the crystallite surface of the adsorbent by phosphate ions.

3.2 Adsorption of Phosphates and the Effects of Experimental Parameters

The adsorption experiments examined the Ag/CaO-AC nanocomposite for the removal of phosphate ions from aqueous solutions. The effects of adsorbent dose, initial phosphate concentration, contact time, and solution pH were varied. The specific effect of individual parameters was examined critically and studied practically. The experimental findings of the research confirmed the expected affinity of the Ag/CaO-AC nanocomposite for phosphate ions in aqueous solutions.

3.2.1 Effect of Adsorbent Dose

Adsorbent dose and adsorbent/solution ratio are important parameters governing the adsorption efficiency of the batch adsorption process [14]. In studying the effect of adsorbent dose

on phosphate adsorption using Ag/CaO-AC nanocomposite, different adsorbent doses ranged from 0.005 – 0.06 g·L^{-1}, while all other variables were kept constant. Figure 5 indicates the effect of the adsorbent dose on the removal percentage and adsorption capacity of the initial phosphate concentration of 10 mg·L^{-1} of phosphate.

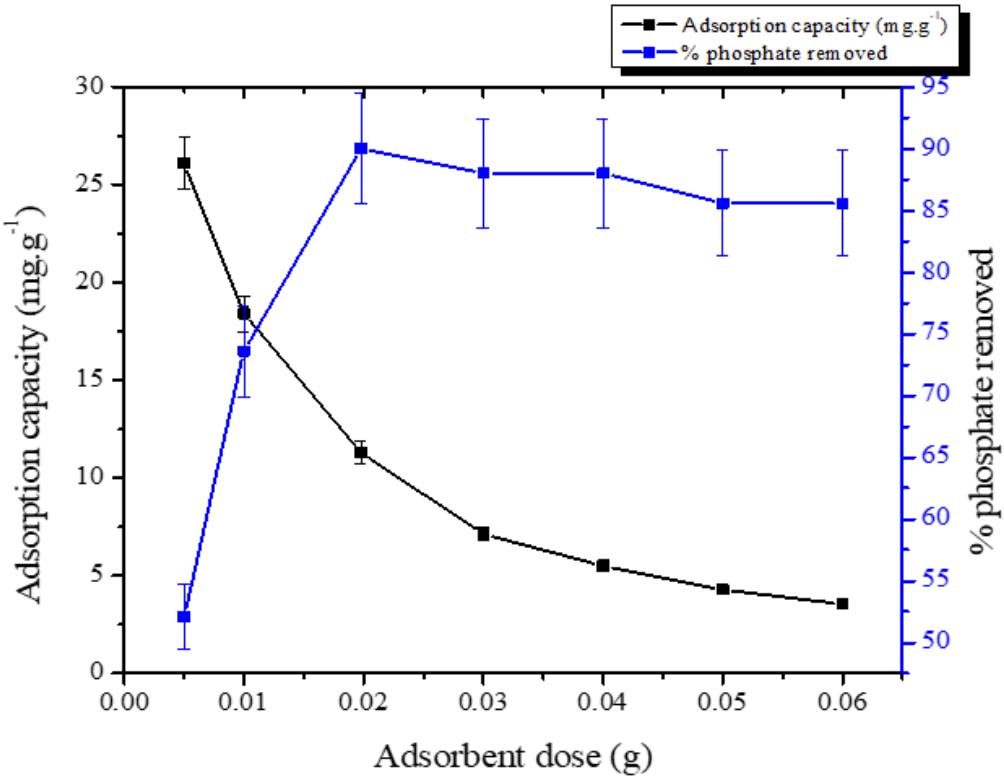

Figure 5 Effects of adsorbent dose on phosphate removal by Ag/CaO-AC nanocomposite. The black symbols represent the trend of the adsorption capacity of the nanocomposite, while the blue symbols represent the percentage of phosphate removed by the nanocomposite.

The maximum removal percentage of phosphate was obtained at 90.4% at a corresponding adsorbent dosage of 0.02 g·L^{-1} with an adsorption capacity of 11.3 mg·g^{-1}. The initial increase was due to the increased accessible surface area and active surface sites for adsorption as the adsorbent dose was raised from 0.005 – 0.02 g·L^{-1}. Further increase in the amount caused a decrease in the adsorption capacity due to the inverse relationship between the adsorption capacity and the adsorbent's mass, as the adsorbate concentration was kept constant. The observed reduction in the active site of the adsorbent might be due to the aggregation of Ag/CaO-AC particles which caused a reduction in the effective surface area and functional site for phosphate adsorption. Furthermore, at a higher adsorbent dose, the aggregation of the adsorbent at the given initial concentration and volume of solution caused the increased unsaturation of the active sites on the Ag/CaO-AC surface, which led to a decrease in adsorption capacity. This result is similar to other studies that have explained the adsorbent dose's role in the pollutants' adsorption [12].

3.2.2 Effect of Initial Phosphate Concentration

The adsorption process is greatly affected by the initial concentration of the adsorbate. In studying the effect of initial phosphate concentration on the adsorption reaction, the phosphate concentration varied in the range of 10-80 mg·L^{-1} with a fixed dose of 0.02 g of Ag/AC-CaO nanocomposite. Figure 6 shows that the removal percentage of phosphate increased from 85.6% to 88% with increased initial phosphate concentration up to 40 mg·L^{-1}. At a lower initial phosphate concentration, nearly all the phosphate ions are in close interactions with the accessible binding sites on the surface of the adsorbent.

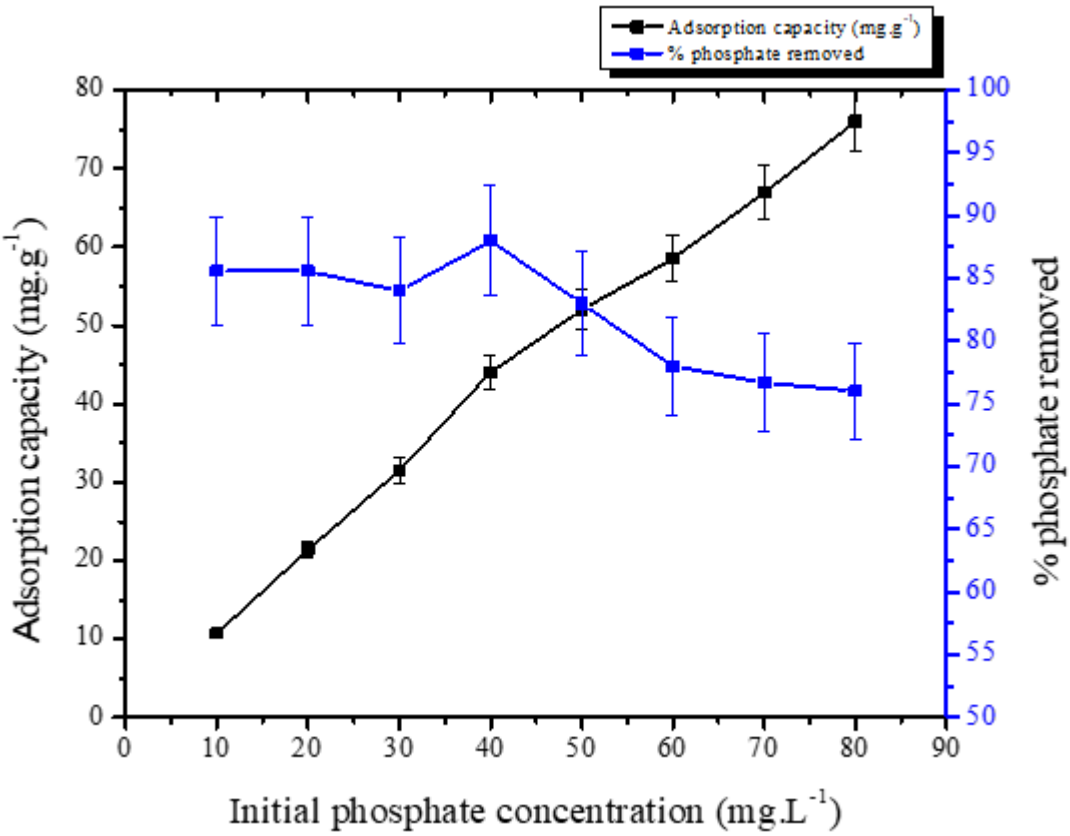

Figure 6 Effects of the initial concentration of phosphate on its removal by Ag/CaO-AC nanocomposite. The black symbols represent the trend of the adsorption capacity of the nanocomposite, while the blue symbols represent the percentage of phosphate removed by the nanocomposite.

On the other hand, the adsorption capacity of the adsorbent increased significantly with the increase in the initial phosphate concentration from 10 to 80 mg·L^{-1}. When the initial phosphate concentration increased, the binding sites of the adsorbent became saturated with the adsorbate. Also, the ratio of the adsorbent's active site to the concentration of phosphate ions decreased, decreasing the removal percentage of phosphate ions. This result is similar to those reported in earlier studies [11, 13]. Additionally, at constant adsorbent mass and volume of adsorbate, the ratio of the active sites of the adsorbent to the concentration of phosphate ions reduced when the initial concentration of phosphate increased. Thus, the reason for the decreased removal percentage of phosphate observed at a higher initial concentration [13].

3.2.3 Effect of Contact Time

The contact time between the adsorbate and adsorbent in a solution is an essential parameter in adsorption because it gives information on the adsorption kinetics of the adsorbent at a given dosage and concentration of the adsorbate [25]. The effect of contact time on the adsorption of phosphate on Ag/CaO-AC was carried out by varying the contact time (15, 30, 45, 60, 75, 90, and 105 minutes), with a fixed initial phosphate concentration of 40 $mg{\cdot}L^{-1}$, and an adsorbent dose of 0.02 g. Figure 7 indicates the effect of contact time on the removal percentage of phosphate and adsorption capacity of Ag/CaO-AC nanocomposite. The removal percentage increased from 48.25% to 94.6%, and the adsorption capacity from 24.13 $mg{\cdot}g^{-1}$ to 47.3 $mg{\cdot}g^{-1}$. Almost 94.6% of phosphate ions were removed within 45 minutes of stirring; the adsorption capacity was stable and only decreased slightly. The amount of phosphate adsorbed by Ag/CaO-AC increased until the equilibrium contact time was reached at 45 minutes, and there was no further increase. At the initial point, adsorption occurred faster due to available active sites on the surface of Ag/CaO-AC. The transfer of external volume controlled the adsorption progression.

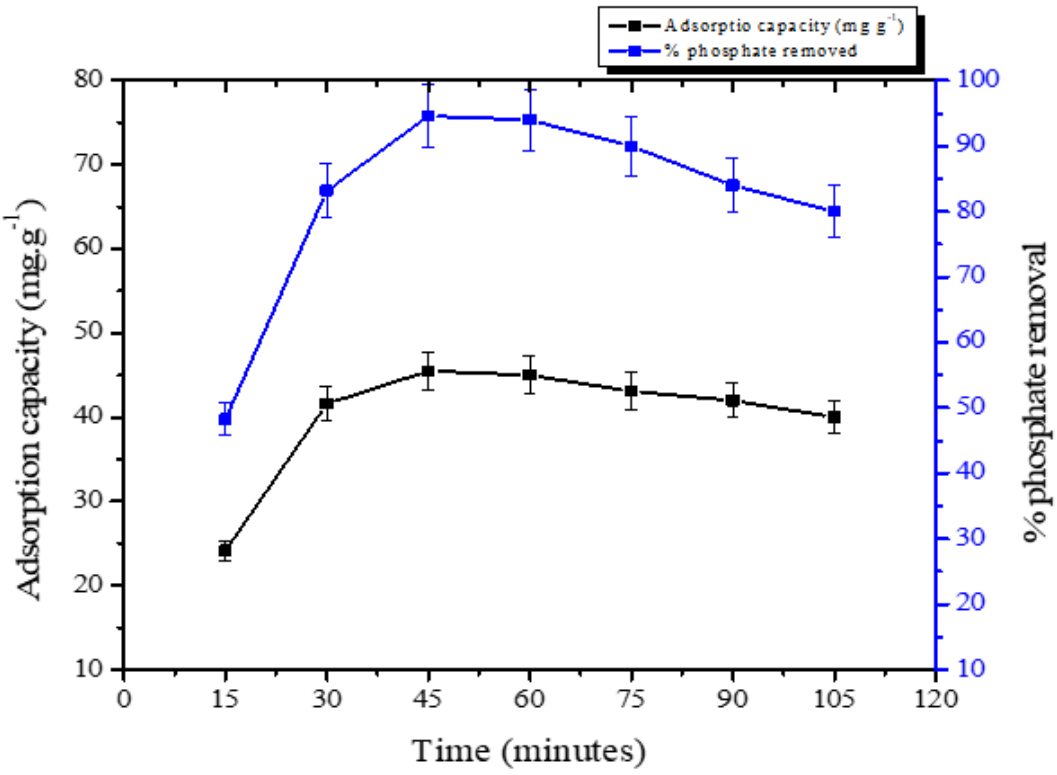

Figure 7 Effects of time on the adsorption of phosphates by Ag/CaO-AC nanocomposite. The black symbols represent the trend of the adsorption capacity of the nanocomposite, while the blue symbols represent the percentage of phosphate removed at various time intervals.

However, as time increased, the active sites on the adsorbent's surface reduced since most active sites were now occupied by the adsorbed phosphate ions [12]. Initially, the faster adsorption capacity was attained due to adsorbate interaction with the adsorbent. After some time, the decreased phosphate removal percentage was observed due to the release of potential ligands from the adsorbent particles in the solution, thereby causing a reduction in phosphate adsorption. A

similar effect of contact time was observed for AgNPs-TAC on phosphate removal [13]. The proposed mechanism for this observation was, first, the saturation of active adsorption sites on the surface of AgNPs-TAC, and second, gradual reduction in the concentration gradient between the bulk solution and the adsorbent.

3.2.4 Effect of pH

The pH of the solution is also an important parameter affecting the phosphate adsorption rate. The effect of pH was varied between 3 to 12 under the following conditions 0.02 g of adsorbent and 40 mg·L^{-1} of phosphate at 45 minutes. Figure 8 displays the effect of pH on phosphate removal using the Ag/CaO-AC nanocomposite. The maximum phosphate removal obtained was at pH 7, with a removal percentage of 99.9 %. This result is similar to the adsorption of phosphate using silver nano-particles-tea activated carbon for phosphate adsorption [13], nanoscale zero-valent iron particles [26], and activated carbon fiber loaded with lanthanum oxide [27]. The effect of pH on phosphate adsorption shows that adsorption is strictly a function of pH. In Figure 8, the adsorption capacity of Ag/CaO-AC decreased from 50 mg·g^{-1} to 33.51 mg·g$^{-1,}$ and the removal percentage dropped from 99.99 % to 67 % as the pH increased from 7 to 11.

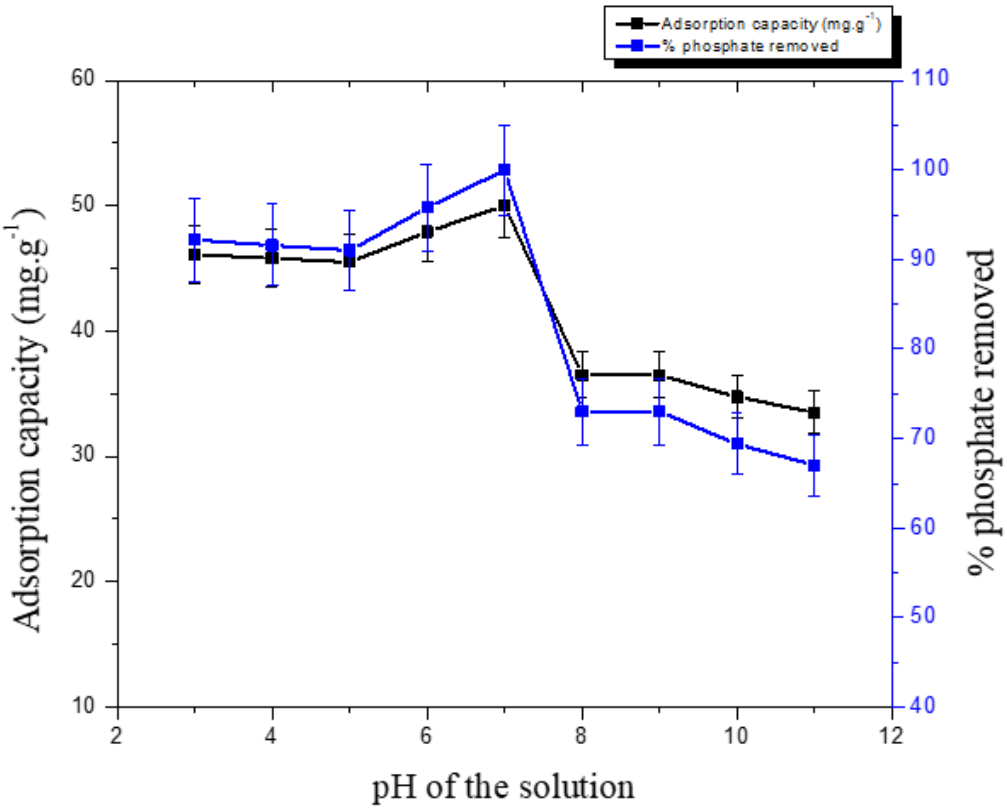

Figure 8 Effects of pH on phosphate removal by Ag/CaO-AC nanocomposite. The black symbols represent the trend of the adsorption capacity, while the blue symbols represent the percentage of phosphate removed.

The percentage removal and adsorption capacity decreased at a pH greater than 7. Phosphates can exist in various forms as H_3PO_4, $H_2PO_4^-$, HPO_4^{2-}, PO_4^{3-} at different pH levels [11, 28, 29]. In an acidic solution, the main phosphate ions are $H_2PO_4^-$ and HPO_4^{2-}, while in alkaline conditions,

phosphate exists mainly as PO_4^{3-} [12]. The pH of the solution can have a critical effect on the adsorption rate because the adsorption of charged phosphate ions changes the surface charge of the adsorbent [4]. The phosphate species present in the solution are observed to be determined by the pH of the solution [30]. At higher solution pH, the adsorption capacity of Ag/CaO-AC nanocomposite decreased due to competition between the OH^- that exists in the solution with the PO_4^{3-} for the adsorption site. Also, a higher concentration of negative charges on the adsorbent surface at higher pH leads to a greater repulsion between the phosphate anions and the negative groups, decreasing phosphate removal. Therefore, as the solution pH increases, a corresponding increase in the fraction of the multi-charged phosphate anions (such as HPO_4^{2-} and PO_4^{3-}) in the solution is observed [29].

3.3 Adsorption Kinetics

Two kinetics models were studied to understand the adsorption behaviors of Ag/CaO-AC nanocomposite on phosphate removal: the pseudo-first-order and the pseudo-second-order models. In addition, kinetics studies helped propose whether the interaction was chemisorption (chemical reaction) or physisorption (mass transfer) and describe the phosphate adsorption rate.

3.3.1 Pseudo-First-Order Kinetic Model

The Pseudo-first-order kinetic model describes the rate of change that occurs in adsorbate uptake at a particular time to be directly proportional to the difference in the saturation concentration and the amount of adsorbate removed with time. It assumes that the phosphate ions removal rates are associated with the quantity of the vacant adsorptive sites. The first-order Lagergren model is represented by Equation 4.

$$\log(q_e - q_t) = \log(q_e) - \frac{k_1}{2.303}t \quad (4)$$

where q_e is the adsorption capacity at equilibrium (mg/g), q_t is the adsorption capacity at time *t* (mg/g) of Ag/CaO-AC nanocomposite, and k_1 is the first-order rate constant min^{-1}. The plot of $\log(q_e - q_t)$ versus t gives a linear relationship from which k_t and q_e can be determined from the slope and intercept of the plot (Figure 9a). The resultant values of the k_1 and r^2 for the pseudo-first-order are shown in Table 1.

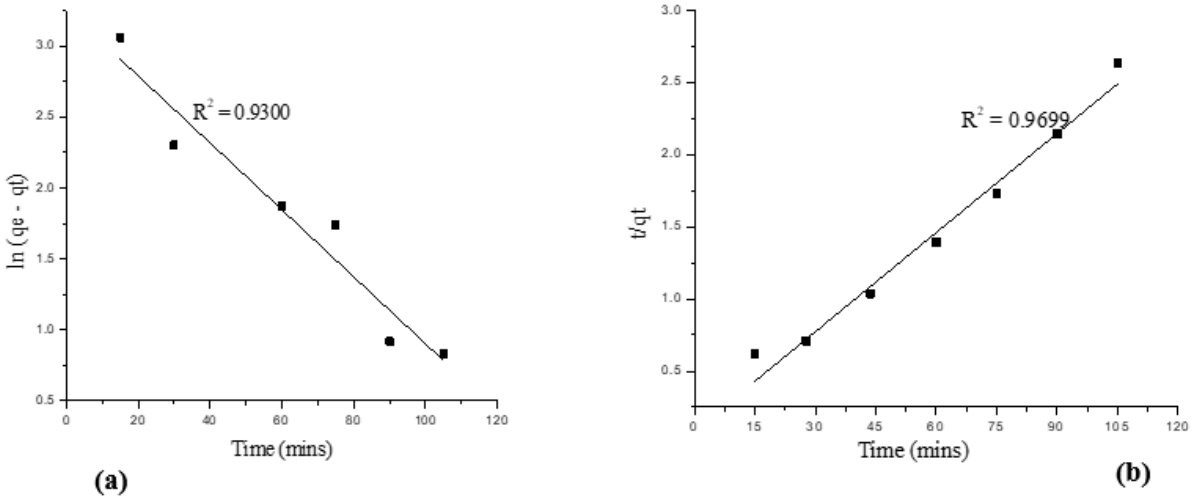

Figure 9 Adsorption kinetics models of phosphate adsorption of Ag/CaO-AC nanocomposite (a) pseudo-first-order and (b) pseudo-second-order kinetics model of phosphate adsorption on Ag/CaO-AC nanocomposite.

Table 1 Adsorption kinetic parameters with correlation coefficient values for the pseudo-first-order and pseudo-second-order kinetic models showing that the pseudo-second-order kinetic model gave the best fit for the phosphate adsorption onto Ag/CaO-AC nanocomposite.

Pseudo-first-order		**Pseudo-second-order**			$q_{e,\ experimental}$ **(mg·g^{-1})**
k₁ (min^{-1})	***r²***	***r²***	***k₂ (g·mg^{-1}min^{-1})***	***q_e (mg·g^{-1})***	
0.0236	0.9300	0.9699	0.006	43.71	45.5

3.3.2 Pseudo-Second-Order Kinetic Model

The pseudo-second-order kinetic model measures the adsorbate adsorbed at time t, and that adsorbed at equilibrium on the surface of the adsorbent [14]. It is given by Equation 5.

$$q_t = \frac{q_e^2 k_2 t}{1 + q_e^2 k_2 t} \quad (5)$$

where q_e is the adsorption capacity at equilibrium (mg·g^{-1}), q_t is the adsorption capacity at time t (mg·g^{-1}), k_2 is the second-order rate constant, g·mg^{-1}min^{-1}. In Figure 9b, the t/q_t vs t plot was used to determine k_2, q_e, and r^2. The calculated values of the qe (mg·g^{-1}) and the second-order rate constants k_2 (g·mg^{-1}min^{-1}) were obtained from the slope and intercept of the plot and are presented in Table 1.

The values of the linear regression coefficient (r^2 from 0.9699 to 0.9300) suggest that phosphate adsorption on Ag/CaO-AC nanocomposite fits the pseudo-second-order kinetic model better than the pseudo-first-order kinetic model. The correlation coefficient of the first-order-model model (r^2 = 0.9300) was somewhat lower than the pseudo-second-order model (r^2 = 0.9699). Moreso, the maximum adsorption capacity [31] calculated from the pseudo-second-order model (43.71 mg/g) was comparatively close to the maximum adsorption capacity obtained from the experiment as opposed to the value obtained from the pseudo-first-order. This result indicates that the pseudo-

second-order kinetics models can describe the adsorption kinetics of phosphate on Ag/CaO-AC. It also suggests that the critical mechanism involved in phosphate adsorption by Ag/CaO-AC nanocomposite is chemical sorption, an exchange of electrons between the adsorbent and phosphate [12].

3.4 Adsorption Isotherms

The adsorption isotherm models describe the adsorption mechanism and relate the adsorbate distribution between the solution and the surface of the adsorbent at equilibrium. The experimental data obtained from the adsorption of phosphate on Ag/CaO-AC were analyzed using two isotherm models, the Langmuir (Equation 6) and Freundlich (Equation 7) isotherm models. The Langmuir model allows accumulation only up to a monolayer. This model assumes that monolayer adsorption occurs on a homogenous or heterogeneous surface and energy of adsorption of all the available active sites is at all times comparable. On the other hand, the Freundlich model presumes the occurrence of multilayer adsorption on a heterogenous surface, thus describing that all the adsorption locations possess different affinities.

$$q_t = \frac{q_e K_L C_e}{1 + K_L C_e} \tag{6}$$

$$q_t = K_F C_e^{\frac{1}{n}} \tag{7}$$

where q_t (mg·g^{-1}) and q_e (mg·g^{-1}) are the maximum adsorption capacity and adsorption capacity at equilibrium, C_e (mg·L^{-1}) is the adsorbate concentration at equilibrium, K_L (L·mg^{-1}) is the Langmuir constant, K_F (mg·g^{-1}) is the Freundlich constant, which indicates the strength of adsorption.

Figure 10 indicates the fitting of the experimental data obtained from phosphate adsorption on Ag/CaO-AC nanocomposite by the Langmuir and Freundlich isotherm models. The results showed that the adsorption data fitted well to Langmuir isotherm with coefficient values (R^2) of 0.9995. On the other hand, the Freundlich isotherm with R^2 of 0.9459 showed less fitting with the experimental data when compared with the Langmuir as presented in Table 2. These data show that the Langmuir isotherm model fits better than the Freundlich isotherm model for phosphate adsorption on Ag/CaO-AC nanocomposite with a monolayer adsorption capacity of 77.4 mg·g^{-1}. Also, the calculated q_e values obtained for the Langmuir were 77.4 mg·g^{-1}, which is close to the experimental value (76 mg·g^{-1}). The result indicates that the adsorption mechanism of Ag/CaO-AC nanocomposite occurred on a monolayer surface or through a fixed number of identical sites on the Ag/CaO-AC surface. Table 3 summarizes the comparative evaluation of the adsorption capacities of phosphate onto different adsorbents. The adsorbent prepared in this study showed a relatively high adsorption capacity compared to some other adsorbents that have been studied.

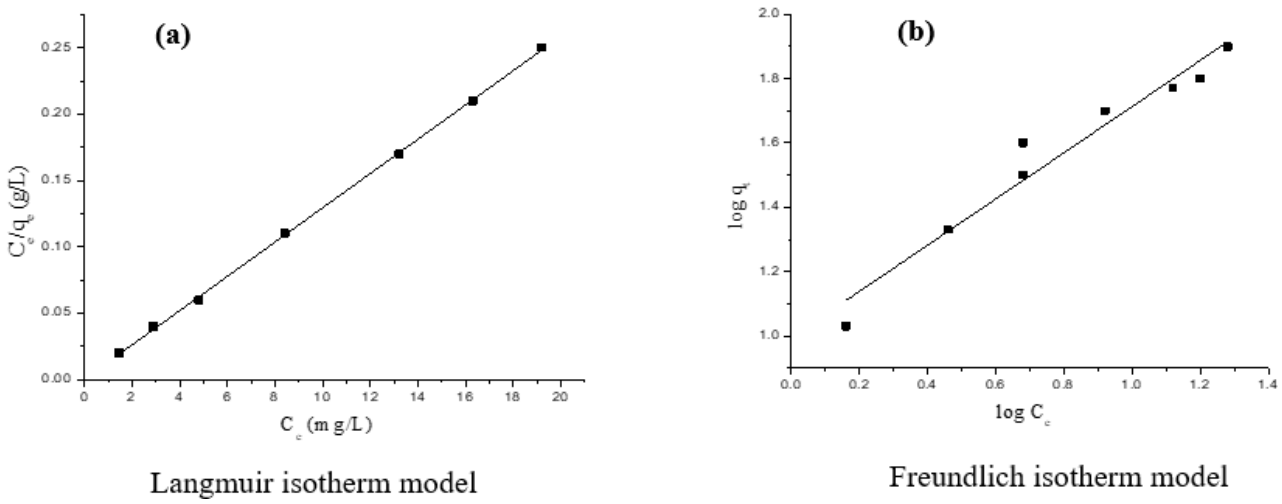

Figure 10 Linear adsorption isotherm models of phosphate adsorption on Ag/CaO-AC nanocomposite to explain the adsorption mechanism. (a) Langmuir isotherm and (b) Freundlich isotherm.

Table 2 Adsorption isotherm parameters and correlation coefficients of the Langmuir and Freundlich isotherm models for the adsorption of phosphate on Ag/CaO-AC nanocomposite.

Langmuir isotherm			**Freundlich isotherm**			$q_{e,\ experimental}$ **(mg/g)**
K_L	R^2	q_e, **(mg/g)**	*1/n*	R^2	K_F	
0.0026	0.9995	77.4	0.7181	0.9459	9.89	76

Table 3 Comparison of phosphate adsorption capacities of different adsorbent materials.

Adsorbent	**Adsorption capacity (mg·g^{-1})**	**References**
AgNPs-TAC [13].	13.62	[13]
Zn Fe/Si MCM-41[32].	97	[32]
Calcium hydroxide-coated dairy manure-derived biochar [33].	13.6	[33]
Zeolite [34].	84.4	[34]
This study	77.4	

4. Mechanism of Phosphate Adsorption

The adsorption mechanism of phosphate on Ag/CaO-AC nanocomposite could be chemical adsorption (Scheme 1). The suggested mechanism for the phosphate adsorption onto this material is ligand exchange between phosphate ions and the hydroxide groups fixed on the surface of the adsorbent [35]. The phosphate adsorption was higher at acidic pH owing to the increased positive charge on the activated carbon surface due to the excess of protons (H^+). The activated carbon surface with some positive charge possesses numerous hydrogen ions, which became released into the solution during adsorption at acidic pH. The adsorbent's increased surface charge supported the

phosphate ions' attachment by electrostatic attraction [35]. At higher pH, a negative functional group of OH^- on the surface of the adsorbent caused the repulsion of anionic phosphate ions, reducing the percentage removal of phosphate from the solution. The identification of phosphate species on the surface of the Ag/CaO-AC after the analysis of the samples by SEM/EDS was also a confirmation of the ion exchange mechanism of phosphate adsorption on the Ag/CaO-AC nanocomposite.

5. Treatment of Real Wastewater Sample

The results showed good phosphate adsorption from an aqueous solution using Ag/CaO-AC nanocomposite. It further served as a basis for further testing the adsorbent's ability to remove phosphate from real wastewater samples collected from the Lubigi Sewage Treatment Plant. The pH of the real wastewater sample, the electrical conductivity, and the phosphate amount were measured, and the respective values obtained were 7.3, 5070 $\mu S \cdot cm^{-1}$, and 30 $mg \cdot L^{-1}$ for phosphate, respectively. The experiment achieved 90.6% of phosphate removal in the wastewater. The result shows that the new Ag/CaO-AC nanocomposite can be an adsorbent to remove phosphate from wastewater.

6. Conclusions

The present study focused on the Ag/CaO-AC nanocomposite design as an adsorbent for removing phosphate from wastewater. Experimental findings showed that the experimental parameters significantly affected the removal percentage and adsorption capacities. Phosphate adsorption was reduced with increased adsorbent dose, increased initial phosphate concentrations, and extended time. Lower pH favored the adsorption more than a higher pH. The result shows that phosphate adsorption was pH controlled and at optimum pH = 7, adsorbent dose = 0.02 g, initial phosphate concentration = 40 $mg \cdot L^{-1}$, and contact time = 45 minutes. The adsorption process fitted well with the Pseudo-second-order kinetic and Langmuir isotherm models through chemisorption and monolayer adsorption. Silver and calcium ions on the activated carbon's surface increase the activated carbon's positive surface charge. It blocks some negative charges that may be present in the activated carbon. Since the adsorbent showed good phosphate removal efficiency on real wastewater samples, this qualifies its application in removing phosphate from wastewater. From this study, it is therefore recommended that desorption studies that will focus on the regeneration of the adsorbent and the recovery of the phosphates are needed. In addition, more studies should focus on recycling the adsorbate (phosphate) for the agricultural production of fertilizers.

Author Contributions

All the authors presented in this research article made a substantial contribution to the design of the research, revising it critically for important content and structure, and gave their approval for this version of the paper to be published.

Funding

This research is part of the project, which is supported by the African Water Resources Mobility Network (AWaRMN) of the Intra-Africa Academic Mobility Scheme funded by the European Union to Usman.

Competing Interests

The authors whose names are registered in the present paper certify that they have NO affiliations with or involved with any organization or entity with any financial interest (such as educational grants; honoraria; membership, employment, consultancies, stock ownership, or other equity interest; participation in speakers' bureaus; and expert testimony or patent-licensing arrangements) or non-financial interest (such as affiliations, personal or professional relationships, knowledge or beliefs) in the subject matter or materials discussed in this paper.

Additional Materials

The following additional materials are uploaded at the page of this paper.

1. Scheme 1: Phosphate adsorption mechanism.

References

1. Liu M, Liu X, Wang W, Guo J. Phosphorus removal from wastewater using electric arc furnace slag aggregate. Environ Technol. 2022; 43: 34-41.
2. Cepan C, Segneanu AE, Grad O, Mihailescu M, Cepan M, Grozescu I. Assessment of the different type of materials used for removing phosphorus from wastewater. Materials. 2021; 14: 4371.
3. Shamshiri A, Alimohammadi V, Sedighi M, Jabbari E, Mohammadi M. Enhanced removal of phosphate and nitrate from aqueous solution using novel modified natural clinoptilolite nanoparticles: Process optimization and assessment. Int J Environ Anal Chem. 2020; 102: 5994-6013.
4. Akram M, Xu X, Gao B, Wang S, Khan R, Yue Q, et al. Highly efficient removal of phosphate from aqueous media by pomegranate peel co-doping with ferric chloride and lanthanum hydroxide nanoparticles. J Clean Prod. 2021; 292: 125311.
5. Mohajeri P. N and P removal from wastewater: A novel approach by developing innovative media augmented by sequencing batch reactor technology (SBR-CBA): A thesis submitted in partial fulfilment of the requirements for the Degree of Doctor of Philosophy at Lincoln University. Lincoln, New Zealand: Lincoln University; 2020.
6. Vianna MTG, Marques M. Removal of orthophosphates in water by modified carbonate material of biological origin. Linnaeus Eco-Tech '14. 2014. doi: 10.15626/Eco-Tech.2014.049.
7. Zhou Q, Wang X, Liu J, Zhang L. Phosphorus removal from wastewater using nano-particulates of hydrated ferric oxide doped activated carbon fiber prepared by Sol–Gel method. Chem Eng J. 2012; 200: 619-626.
8. Suzaimi N, Goh P, Malek N. Modified-nano-adsorbents for nitrate efficient removal: A review. J Appl Membr Sci Technol. 2019; 23. doi: 10.11113/amst.v23n2.161.

9. Yin Q, Ren H, Wang R, Zhao Z. Evaluation of nitrate and phosphate adsorption on Al-modified biochar: Influence of Al content. Sci Total Environ. 2018; 631: 895-903.
10. Reddy S, Nagaraddy N, Ramesh Bashetty D, Mise SR. Adsorption of phosphate using laterite soil, black cotton soil and fuller's earth as adsorbents. Int Res J Eng Tech. 2020; 7: 5091-5095.
11. Zhang X, Lin X, He Y, Chen Y, Zhou J, Luo X. Adsorption of phosphorus from slaughterhouse wastewater by carboxymethyl konjac glucomannan loaded with lanthanum. Int J Biol Macromol. 2018; 119: 105-115.
12. Trinh VT, Pham TTH, Van HT, Trinh MV, Thang PQ, Vu XH, et al. Phosphorus removal from aqueous solution by adsorption using silver nanoparticles: Batch experiment. J Hazard Toxic Radioact Waste. 2020; 24: 04020038.
13. Trinh VT, Nguyen TM, Van HT, Hoang LP, Nguyen TV, Ha LT, et al. Phosphate adsorption by silver nanoparticles-loaded activated carbon derived from tea residue. Sci Rep. 2020; 10: 1-13.
14. Darweesh MA, Elgendy MY, Ayad MI, Ahmed AMM, Elsayed NK, Hammad W. A unique, inexpensive, and abundantly available adsorbent: Composite of synthesized silver nanoparticles (AgNPs) and banana leaves powder (BLP). Heliyon. 2022; 8: e09279.
15. Moustafa MT. Removal of pathogenic bacteria from wastewater using silver nanoparticles synthesized by two fungal species. Water Sci. 2017; 31: 164-176.
16. Khodadadi M, Hosseinnejad A, Rafati L, Dorri H, Nasseh N. Removal of phosphate from aqueous solutions by iron nano-magnetic particle coated with powder activated carbon. J Health Sci Technol. 2017; 1: 17-22.
17. Issaian T, Reyes Cuellar JC. Removing phosphate from aquatic environments utilizing Fe-Co/Chitosan modified nanoparticles. Ciencia en Desarrollo. 2020; 11: 101-110.
18. Ghalehkhondabi V, Fazlali A, Ketabi K. Synthesis and characterization of modified activated carbon (MgO/AC) for methylene blue adsorption: optimization, equilibrium isotherm and kinetic studies. Water Sci Technol. 2021; 83: 1548-1565.
19. Fu LM, Hsu JH, Shih MK, Hsieh CW, Ju WJ, Chen YW, et al. Process optimization of silver nanoparticle synthesis and its application in mercury detection. Micromachines. 2021; 12: 1123.
20. Talabani RF, Hamad SM, Barzinjy AA, Demir U. Biosynthesis of silver nanoparticles and their applications in harvesting sunlight for solar thermal generation. Nanomaterials. 2021; 11: 2421.
21. Mehr FP, Khanjani M, Vatani P. Synthesis of nano-Ag particles using sodium borohydride. Orient J Chem. 2015; 31: 1831-1833.
22. Darshana Senarathna DD, Namal Abeysooriya KH, Dunuweera SP, Ekanayake BP, Wijenayake WM, Rajapakse RM. Removal of phosphate from aqueous solutions using chemically synthesized vaterite polymorph of porous calcium carbonate nanoparticles under optimized conditions. J Nanomater. 2020; 2020: 1-15.
23. Kirboga S, Oner M, Akyol E. The effect of ultrasonication on calcium carbonate crystallization in the presence of biopolymer. J Cryst Growth. 2014; 401: 266-270.
24. Jemal K, Sandeep B, Pola S. Synthesis, characterization, and evaluation of the antibacterial activity of Allophylus serratus leaf and leaf derived callus extracts mediated silver nanoparticles. J Nanomater. 2017; 2017: 4213275.
25. Agbovi HK, Wilson LD. Adsorption processes in biopolymer systems: Fundamentals to practical applications. In: Natural Polymers-Based Green Adsorbents for Water Treatment. Amsterdam, Netherlands: Elsevier; 2021. pp. 1-51.

26. Bezza FA, Chirwa E. Removal of phosphate from contaminated water using activated carbon supported nanoscale zero-valent iron (nZVI) particles. Chem Eng. 2021: 84. doi: 10.3303/CET2184010.
27. Zhang L, Wan L, Chang N, Liu J, Duan C, Zhou Q, et al. Removal of phosphate from water by activated carbon fiber loaded with lanthanum oxide. J Hazard Mater. 2011; 190: 848-855.
28. Qiu B, Duan F. Synthesis of industrial solid wastes/biochar composites and their use for adsorption of phosphate: From surface properties to sorption mechanism. Colloids Surf A. 2019; 571: 86-93.
29. Huang W, Chen J, He F, Tang J, Li D, Zhu Y, et al. Effective phosphate adsorption by Zr/Al-pillared montmorillonite: Insight into equilibrium, kinetics and thermodynamics. Appl Clay Sci. 2015; 104: 252-260.
30. Qiu H, Ye M, Zeng Q, Li W, Fortner J, Liu L, et al. Fabrication of agricultural waste supported UiO-66 nanoparticles with high utilization in phosphate removal from water. Chem Eng J. 2019; 360: 621-630.
31. Adejumo AL, Azeez L, Oyedeji AO, Adetoro RO, Aderibigbe FA. Nanostructured and surface functionalized corncob as unique adsorbents for anionic dye remediation. SN Appl Sci. 2020; 2: 1-12.
32. Fathy M, Zayed MA, Mohamed AMG. Phosphate adsorption from aqueous solutions using novel Zn Fe/Si MCM-41 magnetic nanocomposite: Characterization and adsorption studies. Nanotechnol Environ Eng. 2019; 4: 1-12.
33. Choi YK, Jang HM, Kan E, Wallace AR, Sun W. Adsorption of phosphate in water on a novel calcium hydroxide-coated dairy manure-derived biochar. Environ Eng Res. 2019; 24: 434-442.
34. Zhang K, Van Dyk L, He D, Deng J, Liu S, Zhao H. Synthesis of zeolite from fly ash and its adsorption of phosphorus in wastewater. Green Process Synth. 2021; 10: 349-360.
35. Ouakouak A, Youcef L. Phosphates removal by activated carbon. Sens Lett. 2016; 14: 600-605.